

Mechanical Unfolding of Two DIS RNA Kissing Complexes from HIV-1

Pan T. X. Li^{1*} and Ignacio Tinoco Jr²

¹Department of Biological Sciences, University at Albany, SUNY, Albany, NY 12222, USA

²Department of Chemistry, University of California, Berkeley, CA 94720, USA

Received 23 July 2008;
received in revised form
11 January 2009;
accepted 15 January 2009
Available online
22 January 2009

An RNA kissing complex formed by the dimerization initiation site plays a critical role in the survival and infectivity of human immunodeficiency virus. Two dimerization initiation site kissing sequences, Mal and Lai, have been found in most human immunodeficiency virus 1 variants. Formation and stability of these RNA kissing complexes depend crucially on cationic conditions, particularly Mg^{2+} . Using optical tweezers, we investigated the mechanical unfolding of single RNA molecules with either Mal-type (GUGCAC) or Lai-type (GCGCGC) kissing complexes under various ionic conditions. The force required to disrupt the kissing interaction of the two structures, the rip force, is sensitive to concentrations of KCl and $MgCl_2$; addition of 3 mM $MgCl_2$ to 100 mM KCl changes the rip force of Mal from 21 ± 4 to 46 ± 3 pN. From the rip force distribution, the kinetics of breaking the kissing interaction is calculated as a function of force and cation concentration. The two kissing complexes have distinct unfolding transition states, as shown by different values of ΔX^\ddagger , which is the distance from the folded structure to the unfolding transition state. The ΔX^\ddagger of Mal is ~ 0.6 nm smaller than that of Lai, suggesting that fewer kissing base pairs are broken at the transition state of the former, consistent with observations that the Lai-type kissing complex is more stable and requires significantly more force to unfold than the Mal type. More importantly, neither K^+ nor Mg^{2+} significantly changes the position of the transition state along the reaction coordinate. However, increasing concentrations of cations increase the kinetic barrier. We derived a cation-specific parameter, m , to describe how the height of the kinetic barrier depends on the concentration of cations. Our results suggest that Mg^{2+} greatly slows down the unfolding of the kissing complex but has moderate effects on the formation kinetics of the structure.

© 2009 Elsevier Ltd. All rights reserved.

Keywords: kissing RNA; metal ion binding; single molecule; mechanical unfolding; optical tweezers

Edited by D. E. Draper

Introduction

The majority of retroviral particles contain two copies of their viral genomic RNAs.^{1,2} In human immunodeficiency virus 1 (HIV-1), dimerization of viral RNA greatly enhances recombination during reverse transcription, contributing to hypermutation in the viral genome.^{3,4} The crucial site to initiate such dimerization lies in the 5'-untranslated region

of the viral RNA, known as the dimerization initiation site (DIS).³ The DIS of HIV-1 is made up of a single hairpin, with a loop containing a palindromic sequence.^{5,6} DIS hairpins from two viral RNAs can form a kissing complex by base-pairing the loop nucleotides.^{7,8} Once packaged into a single viral particle, this initial viral RNA dimer can evolve into a mature dimer with multiple interactions between the two strands.^{1–3,9} Formation of the initial dimer is critical for viral survival, as evidenced by the fact that mutations in the loop sequence of the DIS hairpin result in significant reduction in viral replication, RNA packaging, reverse transcription, and infectivity.¹

The nine-nucleotide apical loop of the HIV-1 DIS hairpin contains a six-nucleotide palindromic sequence that is capable of forming tertiary kissing base

*Corresponding author. E-mail addresses: panli@albany.edu; itinoco@lbl.gov.

Abbreviations used: HIV-1, human immunodeficiency virus 1; DIS, dimerization initiation site; MMLV, Maloney murine leukemia virus; dsDNA, double-stranded DNA.

pairs with its counterpart (Fig. 1a). This palindromic sequence is highly conserved.⁴ Out of 64 possible combinations of palindromic hexanucleotides, there are only two sequences commonly found in HIV-1 strains: GUGCAC and GCGCGC. The former was first discovered in Mal isolate, and the latter was first discovered in Lai isolate. The Mal DIS kissing sequence is conserved in clades A, C, F, G, and H of the M (major) group HIV-1, as well as in the O (outlying) group virus.¹⁰ The Lai DIS kissing sequence is conserved in clades B and D of the M group virus. Conservation of the DIS kissing sequence is surprising at first glance, since classification of clades in the M group is solely based on the sequence of the envelope (*env*) gene, which is distally located downstream of the DIS hairpin. This observation reemphasizes the crucial role of the DIS kissing complex in the dimerization of viral RNA. Since a single copy of the viral RNA is much less likely to be packaged and to be infective, only dimerized RNAs can pass mutations to the next generation. Consistent with this hypothesis, matching of the DIS kissing sequences, i.e., pairing Mal with Mal, or pairing Lai with Lai, appears to be a major restriction for intersubtype recombination of viral genomes.¹¹

The two DIS kissing complexes are structurally similar. In all crystal structures^{12–15} and recent NMR solution structures,^{16,17} the two hairpins in the kissing complexes are positioned so that the A-form helices of the hairpin stems are in nearly perfect coaxial stacking. The palindromic hexanucleotides from the two hairpin loops form a segment of a right-handed A-form helix. Between the kissing base pairs and the hairpin stem, the six unpaired nucleotides can adopt several conformations, depending on the sequence and crystallographic/solution conditions. However, an early NMR structure showed that the Lai-type kissing complex was bent and that the

kissing base pairs were distorted from A-form geometry seen in the crystal structure.¹⁸ The structural polymorphism could reflect the dynamics of DIS kissing complexes in solution.

The energetics of kissing base pairs and especially their salt dependence are significantly different from those of secondary structures.^{19,20} The Lai DIS kissing complex is formed by six G•C base pairs, whereas that of Mal contains four G•C and two A•U base pairs. Based on the GC percentage of the kissing base pairs, one would predict that the Lai-type kissing complex is more stable than the Mal-type kissing complex. However, the stabilities of the two structures depend differently on Mg^{2+} .^{19–22} In the absence of divalent cations (with ~300 mM KCl), the Lai kissing complex is significantly more stable than the Mal kissing complex. However, in the presence of 5 mM Mg^{2+} , both kissing complexes show similar K_d values in the nanomolar range.²¹ Consistently, the crystal structure of the Mal kissing complex reveals a bound Mg^{2+} unseen in the structure of the Lai kissing complex; this was hypothesized to contribute to the difference in cation dependence.¹²

Mg^{2+} effects on noncatalytic RNA structures are commonly examined by thermal melting or calorimetry.²³ However, Mg^{2+} catalyzes the hydrolysis of RNA at elevated temperatures, and the two HIV DIS kissing complexes are very stable structures that require nearly boiling temperature to be disrupted at high concentrations of Mg^{2+} .²⁰ Moreover, these techniques are best for studying the thermodynamic effects of Mg^{2+} on RNA stability; it is usually difficult and costly to study kinetics of folding. Optical tweezers provide a practical way of applying force to a single RNA molecule and monitoring its structural change in real time. Here, we used this new technique to probe the dissociation of the DIS kissing complexes.

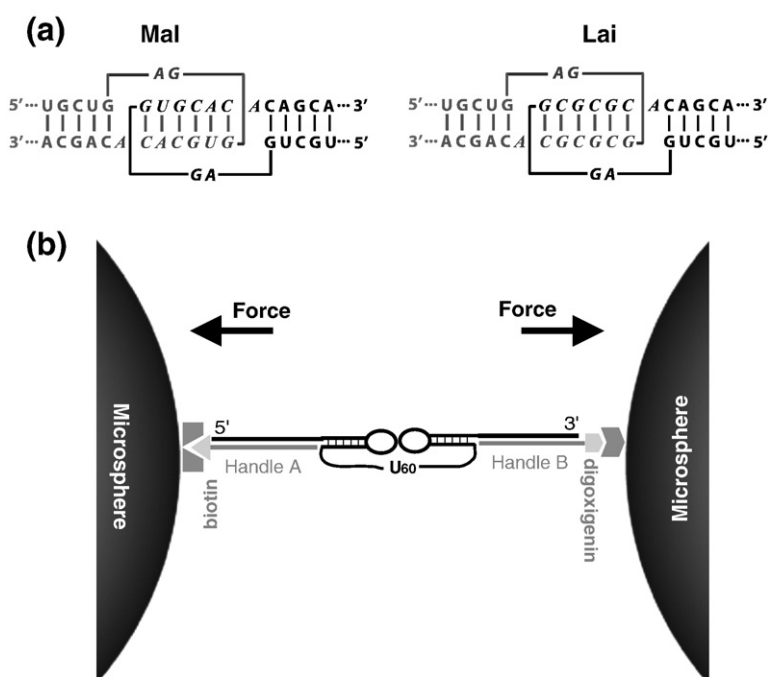


Fig. 1. Experimental design. (a) Mal and Lai types of DIS kissing complexes from HIV-1. The two hairpins are shown in black and gray. Loop sequences are shown in italic letters. (b) A pair of kissing hairpins linked by 60 uracil nucleotides is tethered between two micrometer-sized beads via two dsDNA/RNA handles (a total of ~2.5 kb). An optical trap device was used to manipulate the beads to apply forces in the direction shown by arrows. See Figs. S1 and S2 for more details. The drawing is not drawn to scale.

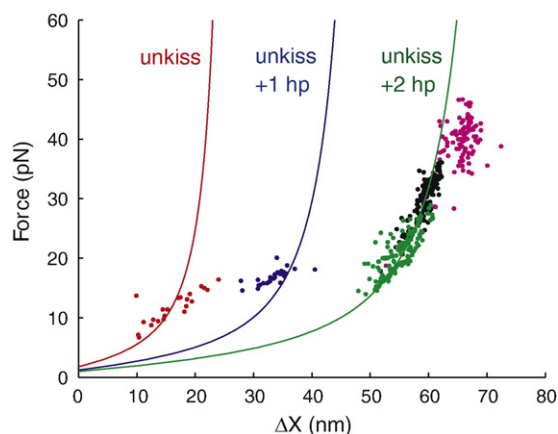


Fig. 3. Force- ΔX relationships of the first transitions in the mechanical unfolding of Mal are computed using a worm-like chain model for RNA (continuous curves; see Fig. S4 for detail). Experimental values of first rips in three-step (red), two-step (blue), and one-step unfolding (green) collected in 100 mM KCl are plotted as dots. The entire RNA always unfolds in a single step in either 1 M KCl (black) or 100 mM KCl with 3 mM $MgCl_2$ (magenta).

of mutant molecules and nanomanipulation methods, we proved that in the MMLV kissing complex, the first unfolding step is always disruption of the kissing interaction (“unkiss”), and that when unkiss occurs at forces higher than the transition forces of the hairpins, breaking of the kiss becomes rate-limiting (Fig. S3). On refolding of the MMLV kissing complex, the two hairpins fold first, followed by formation of the kiss at lower force. Hierarchical mechanical unfolding and refolding were also observed in an adenine riboswitch that contains a kissing complex.³⁸

We performed a series of experiments to test whether the Mal-type kissing complex follows the same unfolding/folding pathways and to rule out the possibility that the first transition is unfolding of one hairpin. First, we pulled individual hairpins. Transition forces and ΔX of individual hairpins are consistent with those of the second and third transitions in the three-step unfolding, as well as with those of the second transition in the two-step unfolding (data not shown). Second, the ΔX values of all observed transitions are consistent with our hypothesis and the structural model. As transitions occur at various forces, we modeled the force- ΔX relationship for unfolding and refolding using a worm-like chain model (Fig. S4).³⁵ Figure 3 shows the force-extension relationship of the unfolding transitions: disruption of the kissing interaction or “unkiss” only (red curve); double transition or breaking of kissing and one of the hairpins together (blue curve); and unfolding of the entire RNA into a single strand in a single step (green curve). Values of experimentally observed first transitions (dots, colored according to type of transition) fit reasonably well with our model. Third, Fig. 3 also shows a wide distribution of the first unfolding forces (7–30 pN), indicating that the rate constant of breaking

the kissing interaction is relatively force-insensitive. In contrast, both hairpins unfold and refold within a 5-pN force range. Most importantly, in all observed traces, hairpins were always unfolded before the force reached 20 pN, confirming that the high rip forces represent the breaking of the kiss. Fourth, we did a “force-jump” experiment²⁸ in which force is rapidly raised from 1 pN to above 25 pN and kept constant (Fig. S5). Hairpins are unstable at such forces, and their lifetimes are estimated to be much less than 1 ms. Yet the entire structure was intact for seconds, followed by a single-step unfolding that increased the extension by ~ 60 nm. Once unfolded, the RNA remained as a single strand for up to 5 min. Only when force is subsequently lowered below 18 pN do refolding and unfolding of hairpins start to appear (Fig. S6). Therefore, as in the MMLV kissing complex, at forces higher than the transition forces of the hairpins, the kissing interaction protects the hairpins from unfolding and the unkiss becomes the rate-limiting first step in unfolding. We thus conclude that the Mal-type kissing complex unfolds by a single pathway despite different force-extension patterns.

We interpret the two zips in the refolding trajectories as the refolding of the hairpins (Fig. 2a–c). Kissing is likely to occur at low force, at which ΔX is too small to be visible in the force-extension curve. To probe the kissing interaction, we lowered the force to different values and pulled again. As shown in Fig. 2d, when the lowest force was kept above 2 pN, the unfolding trajectories show only two rips corresponding to the unfolding of the hairpins, indicating that no kissing complex was formed. This experiment further confirms that disruption of kissing is the first step of unfolding and that kissing only forms after the folding of the hairpins. When force was decreased to between 0.5 and 2 pN, we observed two sets of the unfolding curves: disruption of the kissing interaction and of the hairpins (Fig. 2a–c) and unfolding of only the hairpins (Fig. 2d). As expected, the fraction of the former set of trajectories increases when the lowest force approaches zero. Clearly, the kissing occurs between 0.5 and 2 pN at an unloading rate of ~ 5 pN/s.

We also studied mechanical unfolding of the Lai-type kissing complex under the same conditions. Since Lai and Mal types of kissing complexes are almost identical, except for two nucleotides in each of the hairpin loops, their unfolding and refolding pathways are similar. All force-extension curves of Lai show a single big rip with a ΔX of >55 nm on unfolding and with two zips on refolding. Its rip forces distributed mainly between 30 and 40 pN (Fig. 4). At such high forces, we would also expect the Mal kissing complex to be unfolded into a single strand in a single step (Fig. 3). The rip forces of Lai are significantly higher than those of Mal under the same conditions, consistent with results from thermal melting experiments under similar ionic conditions.^{19,20,39} Notably, the rip force distribution of Mal is about twice as wide as that of Lai (Fig. 4), showing that the unfolding kinetics of the Mal kissing is less force-dependent. We also tested the kissing forces of Lai by

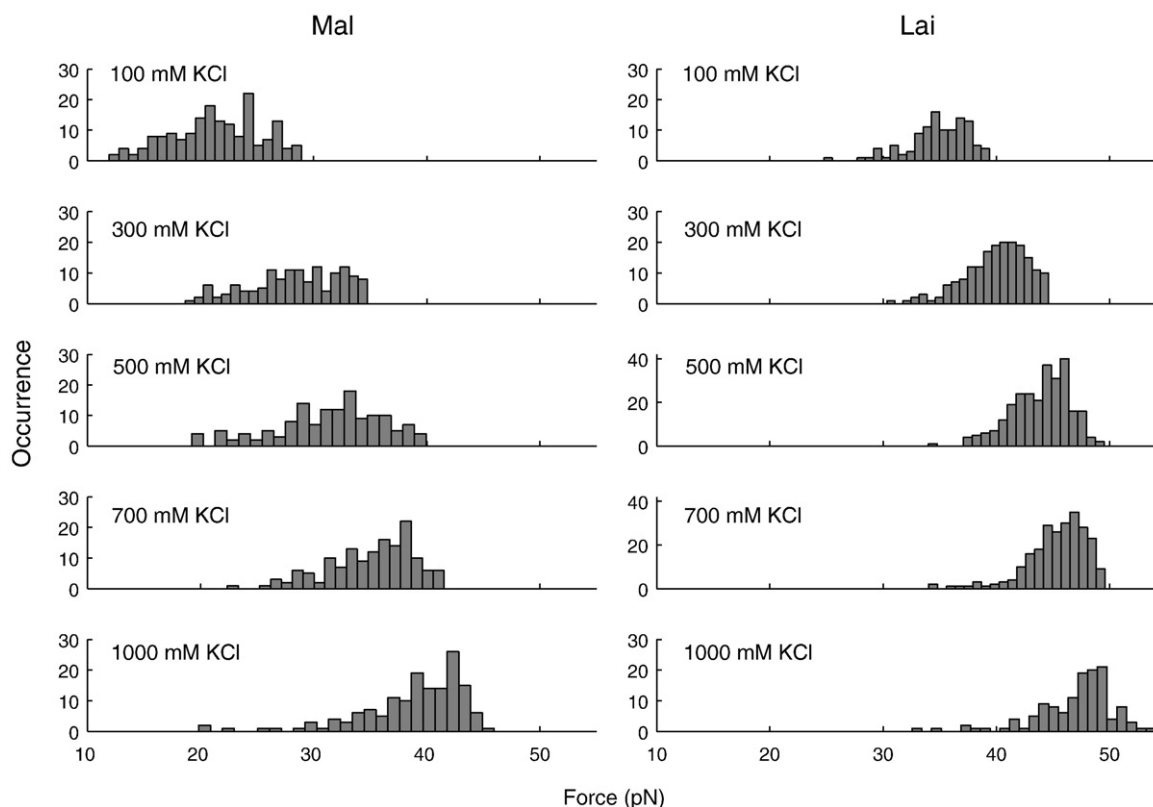


Fig. 4. Effect of KCl on the distribution of first rip (unkiss) forces in unfolding Mal- and Lai-type kissing complexes. Each distribution was split into 20 bins.

lowering force to different values. The kissing forces of Lai range from 1 to 3 pN.

Ionic effects on the rip forces of kissing complexes

The thermal stability of kissing complexes is critically dependent on the ionic strength and type of ions.^{19,20,39} We further examined the mechanical stability of the Mal and Lai kissing interactions in various concentrations of KCl and MgCl₂. As discussed above, we treated the first unfolding transitions as the disruption of the kiss.

When KCl concentration is increased from 100 mM to 1 M, rip forces of both types of kissing complexes increase (Fig. 4). The mean rip force of Mal is ~20 pN in 100 mM KCl and ~40 pN in 1 M KCl. As a comparison, the mean rip force of Lai increases from ~35 pN in 100 mM KCl to ~48 pN in 1 M KCl. Increase in the rip forces also changes the patterns of the unfolding force–extension curves. At and above 300 mM KCl, nearly all curves of Mal display a single big rip similar to the one shown in Fig. 2c. In bulk experiments, Mg²⁺ is more effective than monovalent cations in raising the thermal stability of kissing complexes. Here, we saw a similar effect on the mechanical stability. Adding merely 3 mM MgCl₂ to a solution containing 100 mM KCl raises the mean rip force of the Mal kissing complex by ~25 pN (Fig. 2e), and 1 mM MgCl₂ changes the average rip force of Lai by over 10 pN (Fig. 5).

Previous bulk experiments^{19–21} that covered a wider concentration range of Mg²⁺ showed that 3 mM is slightly below the *K_d* of Mg²⁺ for both kissing complexes. These studies also showed that differences in the thermal stability between Mal and Lai decrease as [Mg²⁺] increases. Although working in low Mg²⁺ concentrations, we observed a similar trend as differences in the rip force of the two kissing structures became narrower at high salt concentrations (Fig. 5).

Ionic effects on the disruption of kissing interactions are more pronounced than on the unfolding/refolding of the hairpins. Addition of 3 mM MgCl₂ increases the unfolding and refolding forces of the hairpins by ~3 pN, but raises the unkiss force by ~25 pN (compare panels a–d with panel e, Fig. 2). We recently found that adding either 10 mM MgCl₂ or 1 M NaCl to RNA hairpins, such as TAR, changes the transition forces by less than 5 pN.⁴⁰ Also, the ionic effect on the formation of the kissing complex from the two hairpins is also comparatively small. The two hairpins appear to kiss at forces between 2 and 3 pN in a solution containing 100 mM KCl and 3 mM MgCl₂. As a result of different ionic effects on unfolding and refolding kinetics, hysteresis between unfolding and refolding force–extension curves increases with ionic strength (Fig. 2).

The force-dependent rip size at high salt concentrations roughly fits the worm-like chain prediction (Fig. 3, black dots), although force–Δ*X* relations in 3 mM Mg²⁺ (magenta dots) appear to be slightly

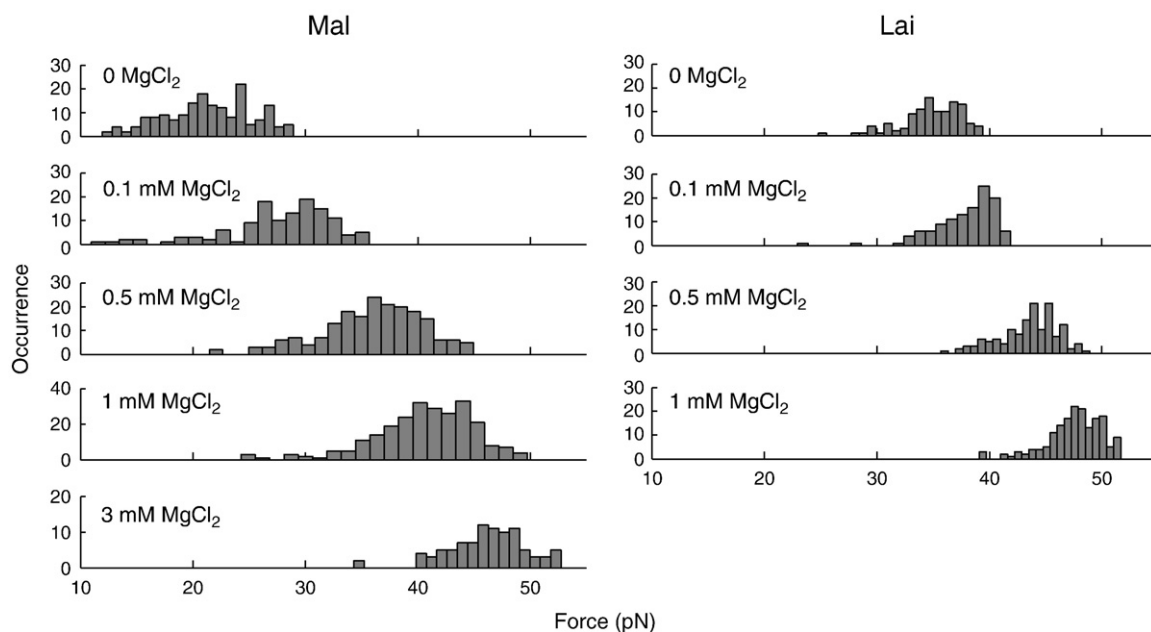


Fig. 5. Effect of MgCl_2 on the distribution of first rip (unkiss) forces in unfolding Mal- and Lai-type kissing complexes. All unfoldings were studied in 100 mM KCl and various concentrations of MgCl_2 . Each distribution was split into 20 bins.

different from predicted values. Ionic strength and type of ions affect mechanical properties of nucleic acids, such as persistence length and contour length.^{41–46} The worm-like chain model we use does not incorporate such effects, since these parameters, especially at high forces, are not available for RNA. We also assumed that the kissing complex is a rigid body that does not change in extension when pulled. However, the kissing complexes may deform under tension. The ends of the dsDNA/RNA handles may also fray at high forces, increasing the apparent rip size. Prediction of ΔX – F relationship will be improved by incorporating these factors.

Force-dependent kinetics of breaking the kissing interactions

The distribution of rip forces reflects the force-dependent unfolding kinetics of a structure. Previously, Evans and Ritchie derived a formula to extrapolate unfolding kinetics from distributions of rip forces:⁴⁷

$$\ln[r \ln[1/N(F, r)]] = \left[k_0 - \ln\left(\frac{\Delta X^\ddagger}{k_B T}\right) \right] + \left(\frac{\Delta X^\ddagger}{k_B T} \right) F \quad (1)$$

in which $N(F, r)$ is the fraction of folded molecule at force F and loading rate r ; k_0 is a factor reflecting both the rate constant at zero force and instrumental factors; ΔX^\ddagger is the distance from the folded state to the transition state; k_B is the Boltzmann constant; and T is the temperature (in kelvins). The linear region of $\ln[r \ln[1/N(F, r)]]$ versus F is usually 10–90% of $\ln[r \ln[1/N(F, r)]]$.^{25,37,48,49} Assuming that disruption of the kissing complex is a single-step process, we fitted the force distribution of breaking the kiss-

ing complexes shown in Figs. 4 and 5 at each ionic condition to Eq. (1) (Fig. 6 and Fig. S7). Values of ΔX^\ddagger and $\ln k_0$ (Tables 1 and 2) were then used to obtain $k_{F, \text{unkiss}}$, the unfolding rate constant at a given force F , using the following equation:

$$\ln k_{F, \text{unkiss}} = F \Delta X^\ddagger / k_B T + \ln k_0 \quad (2)$$

Using this method, we calculated force-dependent unfolding rates of the two kissing complexes under various ionic conditions (a and b in both Figs. 7 and 8). It is obvious from these plots that an increase in both KCl and MgCl_2 changes ΔX^\ddagger only slightly, but significantly decreases the value of $\ln k_0$. Moreover, the ΔX^\ddagger of each structure has a similar value in either KCl or MgCl_2 (Tables 1 and 2). Hence, the

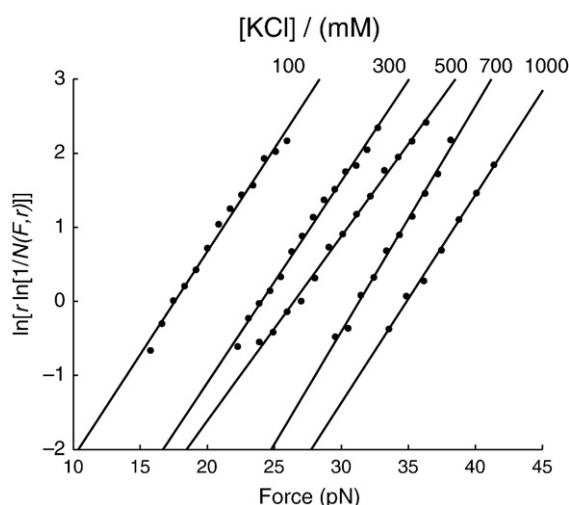


Fig. 6. Kinetic parameters for unfolding the Mal kissing complex were obtained by fitting the distribution of rip forces (Fig. 4) to Eq. (1). See Table 1 for values.

Table 1. Kinetic parameters of unfolding kissing complexes in various concentrations of KCl

[KCl] (mM)	Mal			Lai		
	ΔX^\ddagger (nm)	K_0	n^a	ΔX^\ddagger (nm)	k_0	n^a
100	1.14 ± 0.04	$(2.0 \pm 0.8) \times 10^{-3}$	174	1.91 ± 0.08	$(1.2 \pm 0.8) \times 10^{-7}$	110
300	1.12 ± 0.03	$(4 \pm 2) \times 10^{-4}$	136	1.80 ± 0.02	$(3.4 \pm 0.7) \times 10^{-8}$	186
500	1.02 ± 0.02	$(3 \pm 1) \times 10^{-4}$	141	1.90 ± 0.06	$(3 \pm 1) \times 10^{-9}$	269
700	1.25 ± 0.04	$(2.0 \pm 0.8) \times 10^{-5}$	145	1.98 ± 0.06	$(6 \pm 1) \times 10^{-10}$	239
1000	1.15 ± 0.04	$(1.5 \pm 0.6) \times 10^{-5}$	151	1.72 ± 0.08	$(4 \pm 2) \times 10^{-9}$	128

Values and standard deviations are obtained by fitting force distributions shown in Fig. 4 to Eq. (1).

^a n is the number of collected traces.

distance from the folded state to the transition state is not much affected by the type or the concentration of cations. However, decrease in the y -axis intercept $\ln k_0$ shows that the unfolding kinetics is slowed by increasing concentrations of cations.

The $\ln k$ versus F plots show clearly, but indirectly, the effect of salt. Based on these analyses, we further explored how the unfolding rate depends on the concentration of cations. We estimated the rate constants of unfolding kissing complexes as a function of [KCl] or [MgCl₂] at different forces (c and d in both Figs. 7 and 8). It is well-known that the logarithm of K_{eq} of RNA folding is usually a linear function of the logarithm of cation concentration;^{50,51} however, the effects of salt on kinetics are scarce in the literature. We used the following empirical equations to describe the salt dependence of unkiss rate:

$$\ln k_{F, \text{unkiss}} = m_{\text{KCl}} \ln [\text{KCl}] + \ln k_{0, \text{KCl}} \quad (3)$$

$$\ln k_{F, \text{unkiss}} = m_{\text{MgCl}_2} \ln [\text{MgCl}_2] + \ln k_{0, \text{MgCl}_2} \quad (4)$$

As shown in panels c and d in Figs. 7 and 8, Eqs. (3) and (4) fit the measured data reasonably well.

The unkiss rate constant can be further characterized as a function of both force and salt concentrations. It is relatively straightforward in the case of KCl because ΔX^\ddagger and m_{KCl} are constant in the experimental concentration range of KCl. KCl affects only k_0 in Eq. (2), but not ΔX^\ddagger . Therefore, we can rewrite Eq. (2) as:

$$\ln k_{F, \text{unkiss}} = F \Delta X^\ddagger / k_B T + \ln k_0 = F \Delta X^\ddagger / k_B T + \ln k'_0 + m_{\text{KCl}} \ln [\text{KCl}] \quad (5)$$

in which $\ln k'_0$ is the y -axis intercept when k_F is a rate constant extrapolated to zero force and zero salt

concentration. If we choose a ΔX^\ddagger of 1.1 nm and an m_{KCl} of -2.0 for Mal, $\ln k_0$ is -2.2 . The value of $\ln k_0$ for Lai is -2.1 , with a ΔX^\ddagger of 1.85 nm and an m_{KCl} of -2.3 . We can add another term to the right side of Eq. (5) to account for the effect of MgCl₂:

$$\ln k_{F, \text{unkiss}} = F \Delta X^\ddagger / k_B T + \ln k'_0 + m_{\text{KCl}} \ln [\text{KCl}] + m_{\text{MgCl}_2} \ln [\text{MgCl}_2] \quad (6)$$

When titration of Mg²⁺ is done in the presence of a fixed concentration of KCl, Eq. (6) can be simplified as:

$$\ln k_{F, \text{unkiss}} = F \Delta X^\ddagger / k_B T + \ln k_{0, \text{KCl}} + m_{\text{MgCl}_2} \ln [\text{MgCl}_2] \quad (7)$$

Equation (7) describes Mg²⁺-dependent unkiss kinetics reasonably well (Fig. 8c and d) with a caveat that m_{MgCl_2} may be force dependent. ΔX^\ddagger for each kissing structure is nearly constant (Fig. 8a and b). Values of m_{MgCl_2} , measured in a solution of 100 mM KCl, may not be applied to other ionic conditions because competition between monovalent and divalent metal ions in binding to nucleic acids is thermodynamically complicated.^{50,52}

Discussion

Errors of ΔX^\ddagger

Mechanical pulling experiments are nonlinear processes, and their error propagation has not been well-documented. In a typical experiment, all observations under one condition are pooled together to generate a force distribution (Figs. 4 and 5) from

Table 2. Kinetic parameters of unfolding kissing complexes in various concentrations of MgCl₂

[MgCl ₂] (mM)	Mal			Lai		
	ΔX^\ddagger (nm)	K_0	n^a	ΔX^\ddagger (nm)	k_0	n^a
0.1	1.07 ± 0.05	$(5 \pm 3) \times 10^{-4}$	126	1.80 ± 0.05	$(8 \pm 5) \times 10^{-8}$	119
0.5	1.12 ± 0.02	$(6 \pm 2) \times 10^{-5}$	194	1.81 ± 0.05	$(7 \pm 3) \times 10^{-9}$	140
1	1.20 ± 0.03	$(8 \pm 2) \times 10^{-6}$	248	2.26 ± 0.07	$(8 \pm 5) \times 10^{-12}$	171
3	1.47 ± 0.03	$(9 \pm 2) \times 10^{-8}$	93			

Values and standard deviations are obtained by fitting force distributions shown in Fig. 5 to Eq. (1). KCl (100 mM) is present in all experiments.

^a n is the number of collected traces.

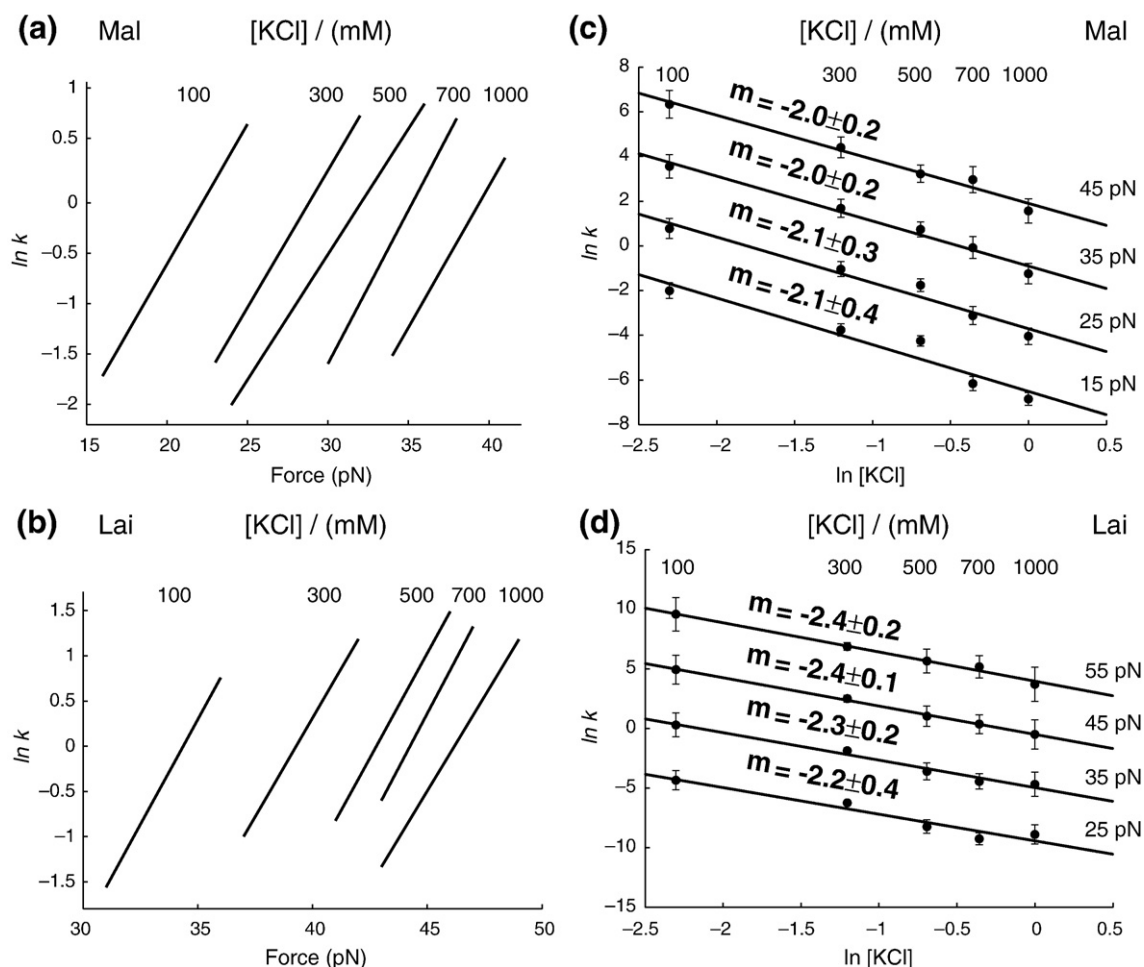


Fig. 7. Effect of KCl on the unfolding kinetics of kissing complexes. (a and b) Force-unfolding rate constants at each [KCl] are calculated using Eq. (2) and parameters in Table 1. The force range of each curve represents $\sim 80\%$ of the rip force distribution. In (c) and (d), unfolding rate *versus* [KCl] at four different forces was calculated using parameters in Table 1 and Eq. (3). Error bars represent a 95% level of confidence. Continuous lines are fitted using Eq. (3). Parameters are summarized in Table 2.

which kinetic parameters are extracted (Fig. 6). The error bars shown in Fig. 6 and the standard deviations shown in Tables 1 and 2 reflect the goodness of fitting force distributions to Eq. (1). The real experimental errors are likely to be larger.

In previous works, we arbitrarily set the threshold for the number of observations to 100, expecting a 10% standard deviation of ΔX^\ddagger .^{24,25,28} Such estimation is consistent with our simulations, which include a force fluctuation of 0.1 pN (data not shown). Following this logic, we expect that errors of ΔX^\ddagger in this study are also about 10%. Hence, we conclude that values of ΔX^\ddagger for breaking each of the two kissing complexes are within the error range (Tables 1 and 2) and, therefore, ΔX^\ddagger of each kissing structure appears not to be affected by cation concentrations.

Experimental limitations

At the highest measured concentrations of MgCl_2 (3 mM for Mal and 1 mM for Lai), ΔX^\ddagger appears to become slightly larger than at lower concentrations.

Under such ionic conditions, both kissing complexes were largely unfolded at >40 pN, with some observations even over 50 pN (Fig. 5). The RNA molecules showed a significantly higher tendency to break their tethering from the beads at >50 pN than at <50 pN. This is likely because the interactions between digoxigenin and antidigoxigenin antibody, by which the molecule is attached to the trapped bead, start to dissociate at about 50 pN. Hence, rip forces over 50 pN were underobserved, and the apparent force distributions under these two ionic conditions were smaller than the true ones. The smaller force distributions in turn resulted in a larger value of ΔX^\ddagger . We also pulled both complexes at higher concentrations of MgCl_2 (up to 10 mM). The molecules broke from beads too often to obtain reliable force distributions. However, it is evident that the kissing complexes become even more stable at these conditions. Many pulling curves showed no rupture at all up to 60 pN, and when a single-step unfolding transition was visible, the rips occurred mostly over 50 pN.

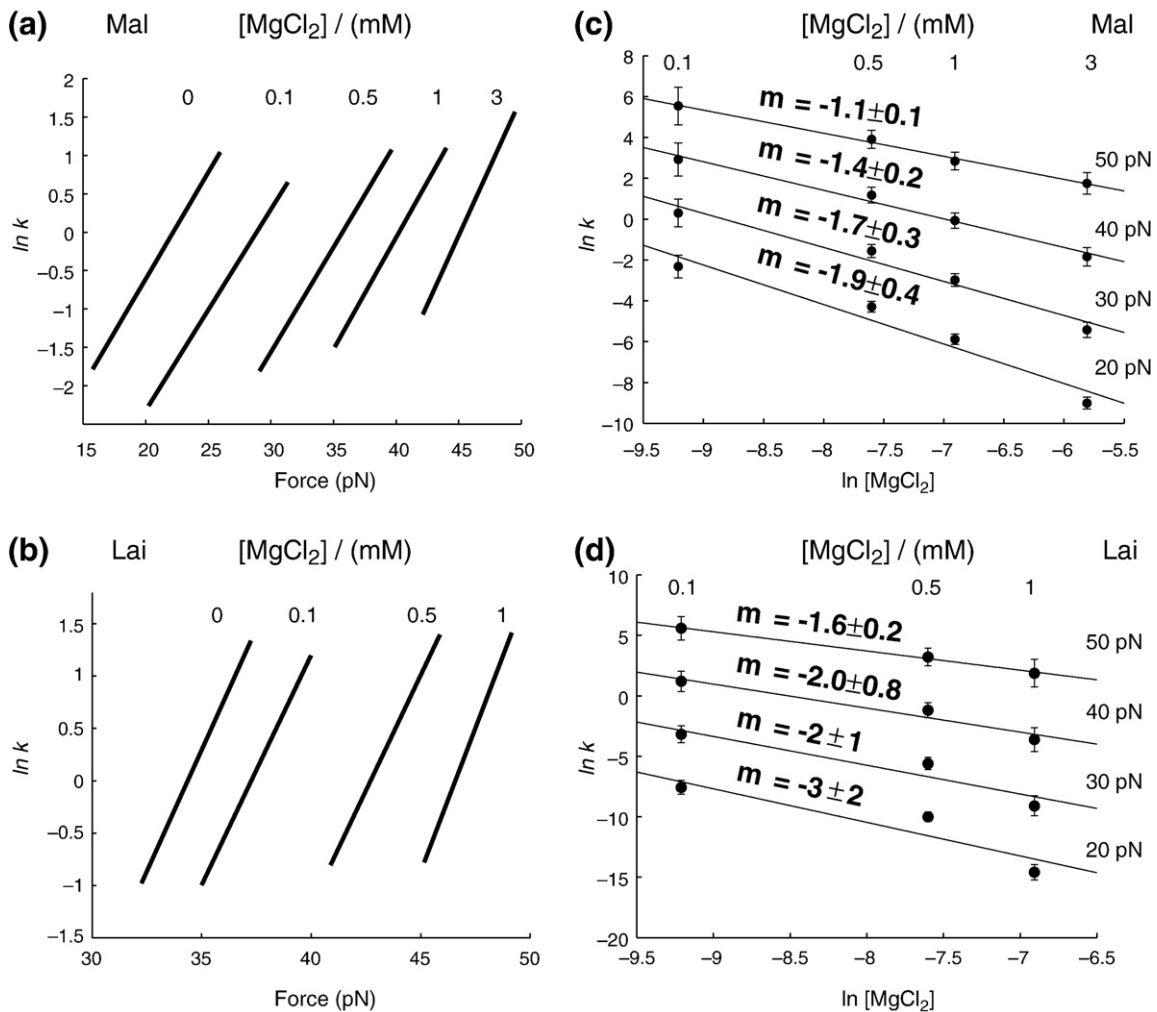


Fig. 8. Effect of MgCl_2 on the unfolding kinetics of kissing complexes. (a and b) Force dependence of unfolding rate constant at various $[\text{MgCl}_2]$. (c and d) Effect of MgCl_2 at four different forces. Continuous lines are fitted using Eq. (4). Parameters are summarized in Table 2.

The tendency for tethers to often break at high forces may also affect the values of m_{MgCl_2} . m_{MgCl_2} shows a decreasing trend as force increases. Because unkiss forces increase rapidly with divalent cations, we have fewer data in MgCl_2 than in KCl ; therefore, the uncertainty of m_{MgCl_2} is larger than that of m_{KCl} . On the other hand, the kissing tends to break at higher forces in a higher concentration of MgCl_2 ; undersampling of high rip forces may also skew the values of m_{MgCl_2} .

Mechanical strength of kissing complexes

We previously studied a minimal kissing complex with only two G•C base pairs.²⁴ Here, we investigated two DIS kissing complexes, both with six kissing base pairs but different sequences. All three kissing complexes show different unfolding forces. Distributions of the unfolding forces and, consequently, values of ΔX^\ddagger are also distinct for each structure (0.65 nm for two base pairs; 1.2 nm for four G•C and two A•U base pairs; and 1.8 nm for six

G•C base pairs). As ΔX^\ddagger describes force-dependent kinetics,^{37,47} the kinetics of the mechanical unfolding of kissing structures clearly depends both on the number and on the sequence of tertiary base pairs.

All three kissing complexes have smaller unkiss ΔX^\ddagger than hairpins (~ 5 nm). Their unkiss force distributions are significantly broader than those of hairpins. Their unkiss rate constants are less force-dependent than those of hairpins. Such difference in the mechanical unfolding of kissing complexes and hairpins likely results from how force is applied to the structure. The three kissing complexes are pulled from opposite ends (Fig. 1b). The direction of applied force approximately overlaps the axis of the kissing helix such that all kissing base pairs are under tension and that more than one base pair is broken at the transition state. In contrast, when a hairpin is “unzipped,” the ripping fork progresses from the bottom of the helix, breaking one base pair at a time (Fig. S8). The difference in how force is applied affects the value of ΔX^\ddagger , rupture force distribution, and force-dependent unfolding kinetics. A

somewhat similar case is mechanical unwinding of dsDNA. A long DNA, such as 48-kbp λ DNA, “melts” at ~ 65 pN when force is applied to the 5'- and 3'-ends on different ends of the DNA.³⁶ When force is applied to 5'- and 3'-ends at the same end of the DNA, the two strands are separated at ~ 15 pN.⁵³ The direction effect is characteristic of mechanical unfolding, distinct from thermal and chemical denaturation.

Physical meaning of ΔX^\ddagger

The distance to the transition state ΔX^\ddagger characterizes the position of the transition state along the reaction coordinate;²³ it reveals whether the transition state is similar to reactant or to product. In simple reactions such as the single-step unfolding of a hairpin, ΔX^\ddagger can be used to interpret the number of base pairs unfolded at the transition state.³⁷ A ΔX^\ddagger of 0.65 nm for breaking the minimal kissing with two base pairs suggests that at the transition state, the end-to-end distance of the molecule has been extended by more than two base pairs.²⁴ Therefore, both kissing base pairs must be disrupted at the transition state. This interpretation is also reasonable to account for the wide rip force distribution and the rip forces as high as 30 pN, which a single base pair is unlikely to withstand. Both Mal and Lai kissing complexes have six tertiary base pairs, and their $\Delta X_{\text{unkiss}}^\ddagger$ values are about 1.2 and 1.8 nm, respectively. The unfolding transition state of Mal is closer to the folded state than that of Lai (Fig. 9a), and fewer base pairs (certainly fewer than six) are broken at the transition state of Mal. Details of the kissing structures at the unfolding transition state are still unclear, given so many possible configurations. If breaking two base pairs yields ΔX^\ddagger of 0.65 nm, Mal and Lai kissing complexes may have

three to four and five to six base pairs broken at their mechanical unfolding transition states, respectively. It is safe to conclude that $\Delta X_{\text{unkiss}}^\ddagger$ and thereby the position of the unfolding transition state along the reaction coordinate depend on both the number and the sequence of kissing base pairs.

A large ΔX^\ddagger also means that more kissing base pairs are broken at the transition state of Lai than of Mal, suggesting a higher kinetic barrier to unfold Lai. Rip forces and unfolding mechanical work are higher for Lai than for Mal. Consistently, values of k_0 for breaking Lai are smaller than those for Mal (Tables 1 and 2), suggesting that at the same force, the kinetic barrier of the unfolding Lai kissing complex is higher (Fig. 9a).

Interestingly, when proteins are mechanically unfolded by atomic force microscopy, the unfolding ΔX^\ddagger is significantly smaller than those for breaking the kissing interactions.⁵⁴ It remains a question whether this difference results from different perturbation methods with very different loading rates (atomic force methods typically use loading rates that are 1 or 2 orders of magnitude higher than rates used with optical tweezers) or it truly reflects the different mechanical properties of proteins and RNA.

Physical meaning of m

To our surprise, K^+ and Mg^{2+} do not affect $\Delta X_{\text{unkiss}}^\ddagger$ much, but significantly decrease the $\ln k_0$ in Eq. (2). Therefore, the metal ions do not change the position of the unfolding transition state along the reaction coordinate, but effectively raise the kinetic barrier relative to the folded state (Fig. 9b). From a different viewpoint, the folded state is greatly stabilized by cations such that the kinetic barrier from the folded state to the transition state is raised. As evident in Eq. (5), m is particularly useful in describing how much the kinetic barrier is increased with ionic concentration.

It is tempting to think that m equals the number of bound ions changed at the transition state. However, such oversimplified explanation may not hold ground. In the KCl titration, concentrations of K^+ and Cl^- are both varied; rigorous treatment of such case is complex and sometimes controversial.⁵¹ In the $MgCl_2$ titration, as the total concentration of Cl^- is dominated by that of KCl, m_{MgCl_2} is closely related to the Mg^{2+} released at the unfolding transition state of kissing. Significantly, m_{KCl} and m_{MgCl_2} for unfolding both kissing complexes are negative, consistent with observations that DNA/RNA helix \rightarrow coil transitions are associated with metal ion release^{41,55} and that cations stabilize the kissing structures thermodynamically.^{19–22} It is also clear that Mg^{2+} is more effective than K^+ in stabilizing the two kissing complexes.

Both Mal and Lai kissing complexes release about two K^+ at their unfolding transition states (Fig. 7c and d). Since fewer base pairs are broken at the transition state of Mal, $m_{KCl}/\Delta X_{\text{unkiss}}^\ddagger$ for Mal is higher than that for Lai, suggesting that more K^+ are

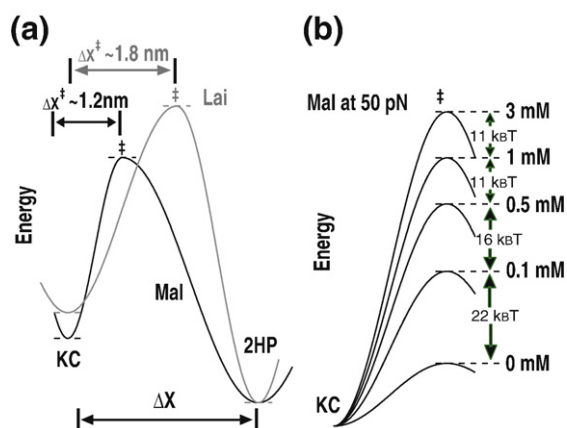


Fig. 9. Unfolding transition state of the two kissing complexes. (a) An illustration of the different unfolding transition states of Mal- and Lai-type kissing complexes. (b) The effect of Mg^{2+} on the height of the kinetic barrier of Mal at 50 pN was calculated using parameters in Table 2. For better comparison, folding energies of the kissing complex under all ionic conditions were arbitrarily set the same.

associated with the Mal-type kissing base pairs broken at its transition state. m_{MgCl_2} values of the two kissing complexes are within the error range (Fig. 8c and d). The physical meaning of $m/\Delta X_{\text{unkiss}}^\ddagger$ remains unclear.

Differences in the mean rip forces of the two kissing complexes become smaller at high concentrations of Mg^{2+} (Fig. 5). Similarly, as the concentration of Mg^{2+} increases, differences in the thermal stability of the two kissing complexes become narrow.^{19–21} Our results suggest that the Mg^{2+} effect on the unfolding kinetics, reflected by m_{MgCl_2} , plays at least a partial role in the convergence of the thermal stabilities of the two kissing complexes at high Mg^{2+} concentrations.

Fast dissociation of cations

If a ligand binds tightly to a receptor, we expect to distinguish the ligand-bound and ligand-free species by two distinct populations of rip forces. In contrast, as the ionic strength increases, the rip force distribution gradually moves toward high force (Figs. 4 and 5). Such moving distribution, analogous to moving peaks in chromatography and ultracentrifugation,⁵⁶ indicates that the structure exchanges multiple metal ions rapidly with the solution. Loosely bound Mg^{2+} also plays a critical role in stabilizing the RNA tertiary structures, as demonstrated by a recent study on an RNA pseudoknot.⁵⁷

Unkiss kinetics at zero force

It is tempting to estimate zero-force unfolding kinetics from mechanical unfolding measurements. In bulk studies, equilibrium dissociation constants for the DIS kissing complexes are a few nanomolars or higher,^{19,20} and association rate constants for kissing complexes are often about $10^6 \text{ M}^{-1} \text{ s}^{-1}$.^{58,59} Hence, the dissociation rate constants should be in the range of 10^{-3} s^{-1} . Mechanical unfolding rates extrapolated to zero force appear to overshoot (Fig. S9). The difference in zero force unfolding rates measured by different methods reflects different mechanisms underlying thermal, chemical, and mechanical denaturation. Also, the bulk experiments measured dimer dissociation, but in our experiment, an intramolecular kissing complex is unfolded.

Thermal stability and mechanical unfolding

Several thermodynamic studies show that the stability of both DIS kissing complexes depends on $[\text{Mg}^{2+}]$.^{19–21} The equilibrium constant of an unfolding reaction can be expressed as the ratio of the unfolding rate to the folding rate. We were not able to quantify the folding free energy because, in our experiments, formation of the kissing interaction was not directly observed. However, by changing the lowest force in pulling experiments, we can find forces that perturb the kissing (Fig. 2d). Mg^{2+} (3 mM) only changes the kissing force of Mal by 1–2 pN, as compared to a >20-pN difference in rip force. The difference is likely because formation of

the kissing interaction involves intramolecular diffusion, whose rate is not as sensitive to electrostatic forces as the unfolding rate. Hence, Mg^{2+} has a larger effect on unkiss than kissing under mechanical tension.

Conclusion

Previous studies established that the Mal and Lai kissing complexes have different thermal stabilities and that Mg^{2+} differentially affects such stabilities.^{19–21} Here we demonstrated that rupture forces of the Lai kissing complex are much higher than those of Mal. This observation indicates that the rate of unfolding of the Lai kissing is much slower than that of Mal at the same force. Moreover, we have found that cations, particularly Mg^{2+} , decrease the unfolding rate of the two kissing complexes. The cation effect is specific both to the type of cation and to the sequence of kissing base pairs. Furthermore, we have shown that neither K^+ nor Mg^{2+} significantly changes the position of the transition state along the reaction coordinate. Instead, cations increase the kinetic barrier. A cation-specific parameter, m , is used to describe empirically how the height of the kinetic barrier depends on the concentration of cations. Also, our results suggest that Mg^{2+} greatly slows down the unfolding of the kissing complex, but has moderate effects on the formation kinetics of the structure.

During translation and viral RNA replication, RNA structures are mechanically disrupted, and their counterions are displaced as molecular machines like helicases, and ribosomes translocate along the RNA.^{60,61} Mg^{2+} ions play two opposite roles: they not only stabilize RNA structures but also enhance nucleotide triphosphatase activity of the molecular machines. Metal ions can affect pause, rate, and direction of translocation by the motors.⁶² Salt-dependent unfolding kinetics is crucial to the functions of RNA-based molecular motors, and our study is a step toward such understanding.

Materials and Methods

Preparation of RNA

Mal and Lai sequences were cloned between the SmaI site in pUC57 vector by Genscript (Piscataway, NJ). Sequences flanking the insert (1.3 kb upstream and 1.2 kb downstream) were used as handles. Preparation of the molecule shown in Fig. 1 was described in detail previously.^{24,25,28} Briefly, a transcription template, including a T7 promoter, handles, and the kissing structure, is generated by PCR from the plasmids. Then RNA of about 2.6 kb was transcribed *in vitro* by T7 RNA polymerase. Two dsDNA handles were also made by PCR. The DNA handle upstream of the kissing structure was biotinylated at the 3'-end, and the downstream DNA handle contained a digoxigenin group at the 5'-terminus. The annealed molecule can be attached to a pair of beads coated with streptavidin and antidigoxigenin antibody, respectively (Fig. 1).

Optical tweezers

Dual-beam optical tweezers were used to study the folding of the kissing complexes.³³ The antidigoxigenin-coated bead was held by a force-measuring optical trap in a flow chamber. The streptavidin-coated bead was mounted on the tip of a micropipette by suction. The extension of the molecule was changed by moving a piezoelectric flexure stage on which the micropipette was mounted (Fig. S1). Force is measured by the spring constant of the trap and the distance of the trapped bead from the center of the trap. Change in the extension of the molecule was measured by relative movements of the trapped bead and the piezoelectric flexure stage. The force and extension of the molecule were recorded at a rate of 100 Hz.

Folding experiments

All unfolding/refolding experiments were done at 22 ± 1 °C. Various concentrations of MgCl₂ were added to a solution containing 10 mM Hepes (pH 8.0) and 100 mM KCl. In titration of KCl, all solutions had 10 mM Hepes (pH 8.0).

Acknowledgement

We thank Dr. Wei Cheng, Dr. Gang Chen, and Dr. Jin-Der Wen for suggestions and comments on the manuscript. This work was supported by National Institutes of Health grant GM-10840 (I.T.) and a grant from University at Albany (P.T.X.L.).

Supplementary Data

Supplementary data associated with this article can be found, in the online version, at [doi:10.1016/j.jmb.2009.01.023](https://doi.org/10.1016/j.jmb.2009.01.023)

References

- Paillart, J. C., Shehu-Xhilaga, M., Marquet, R. & Mak, J. (2004). Dimerization of retroviral RNA genomes: an inseparable pair. *Nat. Rev. Microbiol.* **2**, 461–472.
- D'Souza, V. & Summers, M. F. (2005). How retroviruses select their genomes. *Nat. Rev. Microbiol.* **3**, 643–655.
- Greutorex, J. (2004). The retroviral RNA dimer linkage: different structures may reflect different roles. *Retrovirology*, **1**, 22.
- Brunel, C., Marquet, R., Romby, P. & Ehresmann, C. (2002). RNA loop-loop interactions as dynamic functional motifs. *Biochimie*, **84**, 925–944.
- Paillart, J. C., Marquet, R., Skripkin, E., Ehresmann, B. & Ehresmann, C. (1994). Mutational analysis of the bipartite dimer linkage structure of human immunodeficiency virus type 1 genomic RNA. *J. Biol. Chem.* **269**, 27486–27493.
- Skripkin, E., Paillart, J. C., Marquet, R., Ehresmann, B. & Ehresmann, C. (1994). Identification of the primary site of the human immunodeficiency virus type 1 RNA dimerization *in vitro*. *Proc. Natl Acad. Sci. USA*, **91**, 4945–4949.
- Paillart, J. C., Skripkin, E., Ehresmann, B., Ehresmann, C. & Marquet, R. (1996). A loop-loop “kissing” complex is the essential part of the dimer linkage of genomic HIV-1 RNA. *Proc. Natl Acad. Sci. USA*, **93**, 5572–5577.
- Clever, J. L., Wong, M. L. & Parslow, T. G. (1996). Requirements for kissing-loop-mediated dimerization of human immunodeficiency virus RNA. *J. Virol.* **70**, 5902–5908.
- Russell, R. S., Liang, C. & Wainberg, M. A. (2004). Is HIV-1 RNA dimerization a prerequisite for packaging? Yes, no, probably? *Retrovirology*, **1**, 23.
- Renjifo, B. & Essex, M. (2002). HIV-1 subtypes and recombinants. In *AIDS in Africa* (Essex, M., Mboup, S., Kanki, P. J., Marlink, P. J. & Tlou, S. D., eds), 2nd edit., pp. 138–157, Springer, New York.
- Chin, M. P., Rhodes, T. D., Chen, J., Fu, W. & Hu, W. S. (2005). Identification of a major restriction in HIV-1 intersubtype recombination. *Proc. Natl Acad. Sci. USA*, **102**, 9002–9007.
- Ennifar, E., Yusupov, M., Walter, P., Marquet, R., Ehresmann, B., Ehresmann, C. & Dumas, P. (1999). The crystal structure of the dimerization initiation site of genomic HIV-1 RNA reveals an extended duplex with two adenine bulges. *Structure*, **7**, 1439–1449.
- Ennifar, E. & Dumas, P. (2006). Polymorphism of bulged-out residues in HIV-1 RNA DIS kissing complex and structure comparison with solution studies. *J. Mol. Biol.* **356**, 771–782.
- Ennifar, E., Paillart, J. C., Bodlender, A., Walter, P., Weibel, J. M., Aubertin, A. M. *et al.* (2006). Targeting the dimerization initiation site of HIV-1 RNA with aminoglycosides: from crystal to cell. *Nucleic Acids Res.* **34**, 2328–2339.
- Ennifar, E., Walter, P., Ehresmann, B., Ehresmann, C. & Dumas, P. (2001). Crystal structures of coaxially stacked kissing complexes of the HIV-1 RNA dimerization initiation site. *Nat. Struct. Biol.* **8**, 1064–1068.
- Kieken, F., Paquet, F., Brule, F., Paoletti, J. & Lancelot, G. (2006). A new NMR solution structure of the SL1 HIV-1 Lai loop-loop dimer. *Nucleic Acids Res.* **34**, 343–352.
- Baba, S., Takahashi, K., Noguchi, S., Takaku, H., Koyangi, Y., Yamamoto, N. & Kawai, G. (2005). Solution RNA structures of the HIV-1 dimerization initiation site in the kissing-loop and extended-duplex dimers. *J. Biochem.* **138**, 583–592.
- Mujeeb, A., Clever, J. L., Billeci, T. M., James, T. L. & Parslow, T. G. (1998). Structure of the dimer initiation complex of HIV-1 genomic RNA. *Nat. Struct. Biol.* **5**, 432–436.
- Lorenz, C., Piqaneau, N. & Schroeder, R. (2006). Stabilities of HIV-1 DIS type RNA loop-loop interactions *in vitro* and *in vivo*. *Nucleic Acids Res.* **34**, 334–342.
- Weixlbaumer, A., Werner, A., Flamm, C., Westhof, E. & Schroeder, R. (2004). Determination of thermodynamic parameters for HIV DIS type loop-loop kissing complexes. *Nucleic Acids Res.* **32**, 5126–5133.
- Paillart, J. C., Westhof, E., Ehresmann, B., Ehresmann, C. & Marquet, R. (1997). Non-canonical interactions in a kissing loop complex: the dimerization initiation site of HIV-1 genomic RNA. *J. Mol. Biol.* **270**, 36–49.
- Jossinet, F., Paillart, J. C., Westhof, E., Hermann, T., Skripkin, E., Lodmell, J. S. *et al.* (1999). Dimerization of HIV-1 genomic RNA of subtypes A and B: RNA loop structure and magnesium binding. *RNA*, **5**, 1222–1234.
- Li, P. T. X., Viereg, J. & Tinoco, I., Jr. (2008). How RNA unfolds and refolds. *Annu. Rev. Biochem.* **77**, 27.1–24.
- Li, P. T. X., Bustamante, C. & Tinoco, I., Jr. (2006). Unusual mechanical stability of a minimal RNA kissing complex. *Proc. Natl Acad. Sci. USA*, **103**, 15847–15852.

25. Liphardt, J., Onoa, B., Smith, S. B., Tinoco, I., Jr & Bustamante, C. (2001). Reversible unfolding of single RNA molecules by mechanical force. *Science*, **292**, 733–737.
26. Collin, D., Ritort, F., Jarzynski, C., Smith, S. B., Tinoco, I., Jr & Bustamante, C. (2005). Verification of the Crooks fluctuation theorem and recovery of RNA folding free energies. *Nature*, **437**, 231–234.
27. Dumont, S., Cheng, W., Serebrov, V., Beran, R. K., Tinoco, I., Jr, Pyle, A. M. & Bustamante, C. (2006). RNA translocation and unwinding mechanism of HCV NS3 helicase and its coordination by ATP. *Nature*, **439**, 105–108.
28. Li, P. T. X., Collin, D., Smith, S. B., Bustamante, C. & Tinoco, I., Jr (2006). Probing the mechanical folding kinetics of TAR RNA by hopping, force-jump and force-ramp methods. *Biophys. J.* **90**, 250–260.
29. Liphardt, J., Onoa, B., Smith, S. B., Tinoco, I., Jr & Bustamante, C. (2002). Equilibrium information from nonequilibrium measurements in an experimental test of Jarzynski's equality. *Proc. Natl Acad. Sci. USA*, **296**, 1832–1835.
30. Onoa, B., Dumont, S., Liphardt, J., Smith, S. B., Tinoco, I., Jr & Bustamante, C. (2003). Identifying kinetic barriers to mechanical unfolding of the *T. thermophila* ribozyme. *Science*, **299**, 1892–1895.
31. Chen, G., Wen, J. D. & Tinoco, I., Jr. (2007). Single-molecule mechanical unfolding and folding of a pseudoknot in human telomerase RNA. *RNA*, **13**, 2175–2188.
32. Green, L., Kim, C. H., Bustamante, C. & Tinoco, I., Jr (2008). Characterization of the mechanical unfolding of RNA pseudoknots. *J. Mol. Biol.* **375**, 511–528.
33. Smith, S. B., Cui, Y. & Bustamante, C. (2003). Optical-trap force transducer that operates by direct measurement of light momentum. *Methods Enzymol.* **361**, 134–162.
34. Zuker, M. (2003). Mfold web server for nucleic acid folding and hybridization prediction. *Nucleic Acids Res.* **31**, 3406–3415.
35. Bustamante, C., Marko, J. F., Siggia, E. D. & Smith, S. B. (1994). Entropic elasticity of lambda-phage DNA. *Science*, **265**, 1599–1600.
36. Smith, S. B., Cui, Y. & Bustamante, C. (1996). Overstretching B-DNA: the elastic response of individual double-stranded and single-stranded DNA molecules. *Science*, **271**, 795–799.
37. Tinoco, I., Jr, Li, P. T. X. & Bustamante, C. (2006). Determination of thermodynamics and kinetics of RNA reactions by force. *Q. Rev. Biophys.* **39**, 325–360.
38. Greenleaf, W. J., Frieda, K. L., Foster, D. A. N., Woodside, M. T. & Block, S. M. (2008). Direct observation of hierarchical folding in single riboswitch aptamers. *Science*, **319**, 630–633.
39. Lodmell, J. S., Ehresmann, B., Ehresmann, C. & Marquet, R. (2000). Convergence of natural and artificial evolution on an RNA loop-loop interaction: the HIV-1 dimerization initiation site. *RNA*, **6**, 1267–1276.
40. Viereg, J., Bustamante, C. & Tinoco, I., Jr (2007). Measurement of the effect of monovalent cations on RNA hairpin stability. *J. Am. Chem. Soc.* **129**, 14966–14973.
41. Bloomfield, V. A., Crothers, D. M. & Tinoco, I., Jr (2000). Interaction of nucleic acids and water and ions. In *Nucleic Acids: Structures, Properties, and Functions* (Bloomfield, V. A., Crothers, D. M. & Tinoco, I., Jr, eds), pp. 475–528, University Science Books, Sausalito, CA.
42. Baumann, C. G., Smith, S. B., Bloomfield, V. A. & Bustamante, C. (1997). Ionic effects on the elasticity of single DNA molecules. *Proc. Natl Acad. Sci. USA*, **94**, 6185–6190.
43. Dessinges, M. N., Maier, B., Zhang, Y., Peliti, M., Bensimon, D. & Croquette, V. (2002). Stretching single stranded DNA, a model polyelectrolyte. *Phys. Rev. Lett.* **89**, 248102.
44. Maier, B., Bensimon, D. & Croquette, V. (2000). Replication by a single DNA polymerase of a stretched single-stranded DNA. *Proc. Natl Acad. Sci. USA*, **97**, 12002–12007.
45. Seol, Y., Skinner, G. M. & Visscher, K. (2004). Elastic properties of a single-stranded charged homopolymeric ribonucleotide. *Phys. Rev. Lett.* **93**, 118102.
46. Seol, Y., Skinner, G. M., Visscher, K., Buhot, A. & Halperin, A. (2007). Stretching of homopolymeric RNA reveals single-stranded helices and base-stacking. *Phys. Rev. Lett.* **98**, 158103.
47. Evans, E. & Ritchie, K. (1997). Dynamic strength of molecular adhesion bonds. *Biophys. J.* **72**, 1541–1555.
48. Wen, J. D., Manosas, M., Li, P. T. X., Smith, S. B., Bustamante, C., Ritort, F. & Tinoco, I., Jr (2007). Force unfolding kinetics of RNA using optical tweezers: I. Effects of experimental variables on measured results. *Biophys. J.* **92**, 2996–3009.
49. Manosas, M., Wen, J. D., Li, P. T. X., Smith, S. B., Bustamante, C., Tinoco, I., Jr & Ritort, F. (2007). Force unfolding kinetics of RNA using optical tweezers: II. Modeling experiments. *Biophys. J.* **92**, 3010–3021.
50. Draper, D. E., Grilley, D. & Soto, A. M. (2005). Ions and RNA folding. *Annu. Rev. Biophys. Biomol. Struct.* **34**, 221–243.
51. Record, M. T., Jr, Zhang, W. & Anderson, C. F. (1998). Analysis of effects of salts and uncharged solutes on protein and nucleic acid equilibria and processes: a practical guide to recognizing and interpreting polyelectrolyte effects, Hofmeister effects, and osmotic effects of salts. *Adv. Protein Chem.* **51**, 281–353.
52. Woodson, S. A. (2005). Metal ions and RNA folding: a highly charged topic with a dynamic future. *Curr. Opin. Chem. Biol.* **9**, 104–109.
53. Bockelmann, U., Thomen, P., Essevaz-Roulet, B., Viasnoff, V. & Heslot, F. (2002). Unzipping DNA with optical tweezers: high sequence sensitivity and force flips. *Biophys. J.* **82**, 1537–1553.
54. Garcia-Manyes, S., Brujic, J., Badilla, C. L. & Fernández, J. M. (2007). Force-clamp spectroscopy of single-protein monomers reveals the individual unfolding and folding pathways of i27 and ubiquitin. *Biophys. J.* **93**, 2436–2446.
55. Cantor, C. R. & Schimmel, P. R. (1980). Nucleic acid structural transitions. In *Biophysical Chemistry*, vol. III, pp. 1109–1181, W. H. Freeman, New York.
56. Gilbert, G. A. & Jenkins, R. C. (1956). Boundary problems in the sedimentation and electrophoresis of complex systems in rapid reversible equilibrium. *Nature*, **177**, 853–854.
57. Soto, A. M., Misra, V. & Draper, D. E. (2007). Tertiary structure of an RNA pseudoknot is stabilized by “diffuse” Mg^{2+} ions. *Biochemistry*, **46**, 2973–2983.
58. Nordgren, S., Slagter-Jäger, J. G. & Wagner, G. H. (2001). Real time kinetic studies of the interaction between folded antisense and target RNAs using surface plasmon resonance. *J. Mol. Biol.* **310**, 1125–1134.
59. Nair, T. M., Myszka, D. G. & Davis, D. R. (2000). Surface plasmon resonance kinetic studies of the HIV TAR RNA kissing hairpin complex and its stabilization by 2-thiouridine modification. *Nucleic Acids Res.* **28**, 1935–1940.

-
60. Cheng, W., Dumont, S., Tinoco, I., Jr & Bustamante, C. (2007). NS3 helicase actively separates RNA strands and senses sequence barriers ahead of the opening fork. *Proc. Natl Acad. Sci. USA*, **104**, 13954–13959.
 61. Wen, J. D., Lancaster, L., Hodges, C., Zeri, A. C., Yoshimura, S. H., Noller, H. F., Bustamante, C. & Tinoco, I., Jr (2008). Following translation by single ribosomes one codon at a time. *Nature*, **452**, 598–603.
 62. Lohman, T. M., Tomko, E. J. & Wu, C. G. (2008). Non-hexameric DNA helicases and translocases: mechanisms and regulation. *Nat. Rev. Mol. Cell. Biol.* **9**, 391–401.